Ab initio static and molecular dynamics study of 4-styrylpyridine: Structure, energy and reactivity of the cis and trans isomers in the ground state

Lawson Daku, Latevi Max; Linares, Jorge; Boillot, Marie-Laure

CHEMPHYSCHEM

DOI: 10.1002/cphc.200700117

Ab Initio Static and Molecular Dynamics Study of 4-Styrylpyridine**

Latévi M. Lawson Daku,*[a] Jorge Linares,[b] and Marie-Laure Boillot[c]

We report an in-depth theoretical study of 4-styrylpyridine in its singlet S_0 ground state. The geometries and the relative stabilities of the trans *and* cis *isomers were investigated within density functional theory (DFT) as well as within Hartree–Fock (HF), second-order Møller–Plesset (MP2), and coupled cluster (CC) theories. The DFT calculations were performed using the B3LYP and PBE functionals, with basis sets of different qualities, and gave results that are very consistent with each other. The molecular structure is thus predicted to be planar at the energy minimum, which is associated with the* trans *conformation, and to become markedly twisted at the minimum of higher energy, which is associated with the* cis *conformation. The results of the calculations performed with the post-HF methods approach those obtained with the DFT methods, provided that the level of treatment of the electronic correlation is high enough and that sufficiently flexible basis sets are used. Calculations carried out within DFT also allowed the determination of the geometry and the energy of the molecule at the biradicaloid transition state associated with the thermal* cis⇄trans *isomerization and at the transition states associated with the enantiomerization of the* cis *isomer and with the rotations of the pyridinyl and phenyl groups in the* trans *and* cis *isomers. Car–Parrinello molecular dynamics simulations were also performed at 50, 150, and 300 K using the PBE functional. The studies allowed us to evidence the highly flexible nature of the molecule in both conformations. In particular, the* trans *isomer was found to exist mainly in a nonplanar form at finite temperatures, while the rotation of the pyridinyl ring in the* cis *isomer was incidentally observed to take place within ≈1 ps during the simulation carried out at 150 K on this isomer.*

1. Introduction

The stilbenoid compounds,[1,2] which react in the presence of light by undergoing a change in their electronic and geometric structures, have been especially documented, as they are of interest in molecular photochemistry[3] and theoretical[4] studies. In addition to their important role as model compounds of biological phototropic systems,[5,6] they also serve as building blocks for organic materials,[3,7,8] whose properties could be used in optical and electro-optical applications, such as optical data storage, laser dyes, nonlinear optics, or photochemically cross-linked polymers.

The *N*-heteroaromatic analogues, namely, the styrylpyridines (or stilbazoles), can act as *N*-coordinating ligands in transition-metal complexes. It has been established that the photoreactivity of 4-styrylpyridine complexes of Ru^{II}, Re^{I}, and W^{0}[9–12] is dominated by the photoinduced *cis*⇄*trans* isomerization of the 4-styrylpyridine ligand (Figure 1).

The photoinduced isomerization of styrylpyridine ligands has proven to be a means of photoswitching the properties of transition-metal complexes, and thus, photocontrol of the reactivity of porphyrin complexes can be achieved in this way.[13–15] Of more especial interest to us is the application of such an approach to complexes of transition-metal cations, such as Fe^{II} or Fe^{III}, which are likely to exhibit a spin-crossover phenomenon.[16–20] The approach led to the so-called ligand-driven light-induced spin change (LD-LISC) phenomenon,[21–24] in which the optical switching of the photoreactive ligand (namely, the *cis*⇄*trans* photoisomerization of styrylpyridine) causes a change of electronic structure that, in turn, may induce a high-spin⇄low-

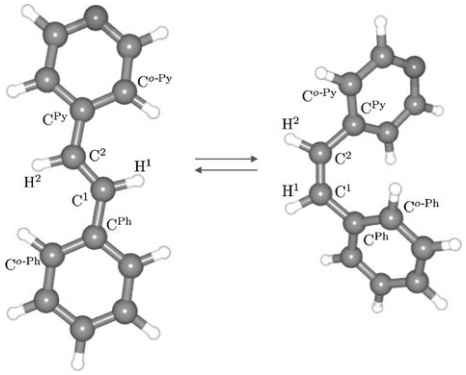

Figure 1. Scheme of the *trans*⇄*cis* isomerization of 4-styrylpyridine. The atom labeling used in the text is also indicated.

[a] *Dr. L. M. Lawson Daku*
Département de chimie physique, Université de Genève
30 quai Ernest-Ansermet, CH-1211 Genève 4 (Switzerland)
Fax: (+41) 22-379-6103
E-mail: max.lawson@unige.ch

[b] *Prof. J. Linares*
Groupe d'Etude de la Matière Condensée, UMR 8635
Université de Versailles Saint-Quentin-en-Yvelines
45 Avenue des Etats-Unis, 78035 Versailles Cedex (France)

[c] *Dr. M.-L. Boillot*
Institut de Chimie Moléculaire et des Matériaux d'Orsay, UMR 8182
Equipe de Chimie Inorganique, Université Paris-Sud
15, rue G. Clémenceau, 91405 Orsay (France)

[**] Structure, Energy, and Reactivity of the *cis* and *trans* Isomers in the Ground State

spin conversion. This approach provides a bistable spin system at a molecular scale and, consequently, it may have potential applications in the field of all-optical, high-density, permanent memories.

The observation of the LD-LISC effect raises different questions concerning the interplay between the metal ion and the photoactive moiety: What are the natures of the excited state(s) and the path(s) involved in the conversion process, and how do they depend on the excitation wavelength? What are the structural and electronic changes at the metal center that result from the *trans*⇄*cis* isomerization of styrylpyridine? How do the latter depend on the spin multiplicity of the transition metal ion? Is there a chance to observe a collective process upon photoexcitation of complexes incorporating several photoactive ligands? To address these issues, time-resolved spectroscopy studies are planned, in which the dynamics of the spin-state change versus the dynamics of the ultrafast photochemical processes will be analyzed.[24] The experimental approaches will not necessarily be able to help us answer all the above questions, but this should be possible with the use of quantum-chemical methods. This is the reason for the theoretical investigation of a prototypical LD-LISC complex, namely, the Fe(4-styrylpyridine)$_4$(NCS)$_2$ complex[22] shown in Figure 2.

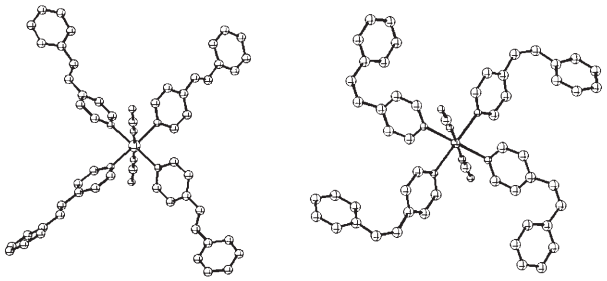

Figure 2. X-ray structures of the iron(II) complexes Fe(*trans*-4-styrylpyridine)$_4$(NCS)$_2$ (left) and Fe(*cis*-4-styrylpyridine)$_4$(NCS)$_2$ (right).[22] The all-*trans* complex exhibits spin crossover while the all-*cis* complex is a high-spin species.

The large number of atoms present in this complex precludes the use of high-level wavefunction-based methods, such as the coupled cluster singles and doubles with perturbative connected triples (CCSD(T))[25] or the multiconfigurational second-order perturbation (CASPT2) methods,[26,27] while those based on density functional theory (DFT)[28–32] can efficiently be applied to such a large system. This has been illustrated by recent DFT studies of iron(II) and cobalt(II) complexes performed within the framework of the phenomenon of spin crossover; (see refs. [33–40], and references therein). In the case of the Fe(4-styrylpyridine)$_4$(NCS)$_2$ LD-LISC complex, we should thus be able to: 1) determine the changes in the geometry, the energy, and the optical properties that accompany the photoswitching of the conformation of one or several 4-styrylpyridine ligands, 2) establish the dependence of these changes on the spin state, and 3) relate them to the changes in the orbital interactions between the constitutive fragments of the complex. In summary, the use of DFT methods should help us obtain a very detailed picture of the LD-LISC phenomenon.

As a mandatory first step towards the study of the whole complex, we carried out an in-depth characterization of the 4-styrylpyridine photoactive moiety within DFT. We thus achieved a very detailed description of its geometry, energetics, and reactivity in the S_0 ground state. These results will be presented below. The remainder of the manuscript is organized as follows: Section 2 gives the computational details, while in Section 3, the ground-state geometries and the relative stability of the two isomers are determined. A comparison is made with the parent stilbene molecule (Section 3.1). To assess the performance of the DFT methods used, the results were compared with those obtained from calculations performed at the Hartree–Fock (HF), second-order Møller–Plesset (MP2), and CCSD(T) levels. This comparison was followed by the determination—on the ground-state potential energy surface (PES)—of the transition states associated with the thermally activated *trans*⇄*cis* isomerization, the enantiomerization of the *cis* isomer, and the rotation of the aromatic cycles in the *trans* isomer (Section 3.2). Finally, temperature effects on the geometries of the *cis* and *trans* isomers are investigated by means of ab initio molecular dynamics (MD) simulations (Section 3.3).

2. Computational Details

Static calculations were performed with the NWChem program package.[41,42] The geometries of the isomers were optimized using the B3LYP hybrid functional[43–45] and the PBE generalized gradient approximation (GGA) functional.[46,47] To probe the influence of the basis sets on the description of the structure and the energetics of the two isomers, these geometry optimizations were carried out with two all-electron Gaussian-type orbital (GTO) basis sets (which we will call *G* and *G*′). For all atoms, *G* consists of the DFT basis set DZVP of double-ζ polarized quality proposed by Godbout et al.[48]. *G*′ differs from *G* by the fact that the N and C atoms are now described by the DFT basis set TZVP of triple-ζ polarized quality.[48] The structural and energetic properties of the two isomers were also determined at the HF and MP2 levels using the correlation-consistent cc-pVDZ double-ζ polarized basis set introduced by Dunning and co-workers.[49–51] The MP2 calculations were carried out within the frozen core approximations. The cc-pVDZ was also used to perform the geometry optimizations at the DFT level, thus allowing a rigorous comparison between the results of the wavefunction-based and DFT methods. These geometry optimizations were followed by a vibrational analysis to ensure that the calculated structures of the two isomers are true minima. The molecular structure of *trans*-4-styrylpyridine is given as nonplanar by the wavefunction-based methods and as planar by the DFT methods. To investigate this issue further, we performed a section of the ground-state PES in the vicinity of the *trans* minimum by doing single-point CCSD(T)/cc-pVDZ calculations on partially relaxed B3LYP/*G*′ geometries. The geometry of the *trans* isomer was also optimized at the MP2/aug-cc-pVDZ level. The transition-state optimizations were per-

formed at the B3LYP/*G* and PBE/*G* levels and followed by vibrational analyses.

Ab initio MD simulations were performed within DFT by using the Car–Parrinello scheme,[52] as implemented in the Car–Parrinello MD (CPMD) program package[53] (the PBE functional was employed). Fully separable,[54] norm-conserving Troullier–Martins pseudopotentials[55] were used to describe the nuclei and the core electrons of all atoms, while the wavefunctions of the valence electrons were expanded in a plane-wave (*P*) basis set, with a kinetic-energy cutoff of 80 Ry. The calculations were carried out on a molecule centered in a cubic box of length = 18 Å by solving Poisson's equation for nonperiodic boundary conditions.[56] According to the results of the geometry optimizations performed with cutoff values of 60, 80, 100, 110, and 120 Ry (data not shown), the kinetic-energy cutoff of 80 Ry allows the convergence of the geometric and energetic properties of both isomers. Furthermore, the results obtained under these conditions for the optimized geometries of the *cis* and *trans* isomers—and for their energy difference—are in good agreement with those obtained from the calculations with the PBE functional and the all-electron basis sets (see below). The CPMD simulations were performed with target temperatures of 50, 150, and 300 K, using a fictitious mass of 500 a.u. and a time step of 4 a.u. (ca. 0.0968 fs) for the integration of the equations of motion. Starting from the optimized geometry of the *cis* or the *trans* isomer, the simulation temperatures were adjusted during a first run (of ca. 0.1 ps) by means of velocity scaling. Then, during the production run (of ca. 2.4 ps), they were controlled by using the Nosé–Hoover chain algorithm[57–62] (that is, one Nosé–Hoover chain was put on each ionic degree of freedom—"massive" thermostating—and another one on the electronic degrees of freedom).

The results of the calculations were visualized and analyzed using the extensible computational chemistry environment (Ecce)[63] and the gOpenMol[64,65] softwares.

3. Results and Discussion

3.1. Geometries and Relative Stabilities of the Two Isomers

3.1.1. Results of the DFT Calculations

For each isomer, the geometries obtained with the PBE and B3LYP functionals, combined with any of the two basis sets (*G* or *G'*), were very similar. To discuss these geometries, we will only consider key structural parameters that help to characterize the rearrangement of the substituents of the ethylenic group around the C^1–C^2 bond upon the *trans*⇔*cis* isomerization, namely, the C^{Ph}–C^1 and C^2–C^{Py} bond lengths, the C^{Ph}–C^1–C^2 and C^1–C^2–C^{Py} angles, the $\tau = C^{Ph}$–H^1–H^2–C^{Py} dihedral angle, and the $\measuredangle$(Py,Ph) angle between the planes defined by the phenyl and the pyridinyl rings. The optimized values of the selected structural parameters are reported in Table 1 along with those of the C^1–C^2 bond length. For each isomer, the values found for a given angle or bond length hardly vary with the theoretical levels. However, the B3LYP and PBE values found for τ and $\measuredangle$(Py,Ph) in the *cis* isomer differ by about 1–2°, which indicates that the two functionals actually give slightly different arrangements of the substituents of the isomerisable C^1–C^2 moiety for this isomer (Table 1).

Table 1. Selected distances [Å] and angles [°] in optimized *trans* and *cis* geometries of 4-styrylpyridine.[a]

	C^{Ph}–C^1	C^1–C^2	C^2–C^{Py}	C^{Ph}–C^1–C^2	C^1–C^2–C^{Py}	τ	$\measuredangle$(Py,Ph)
trans-4-styrylpyridine							
B3LYP/*G*	1.468	1.351	1.468	127.3	126.4	180.0	0.0
B3LYP/*G'*	1.463	1.344	1.463	127.5	126.7	180.0	0.0
PBE/*G*	1.466	1.362	1.465	127.3	126.4	180.0	0.0
PBE/*G'*	1.461	1.355	1.460	127.4	126.6	180.0	0.0
PBE/*P*	1.460	1.352	1.459	127.2	126.5	180.0	0.0
exp[66]	1.466	1.337	1.466	125.8	125.8	179.1	0.0
cis-4-styrylpyridine							
B3LYP/*G*	1.478	1.352	1.477	130.8	130.5	6.6	51.5
B3LYP/*G'*	1.473	1.345	1.472	130.8	130.5	6.4	52.3
PBE/*G*	1.475	1.362	1.474	131.0	130.7	7.5	49.8
PBE/*G'*	1.470	1.356	1.471	130.9	130.7	7.4	50.4
PBE/*P*	1.469	1.353	1.469	130.7	130.5	8.0	51.0

[a] The values found for these parameters in the X-ray structure of the *trans* isomer are reported for comparison.

The *trans* isomer was found to be planar, independent of the theoretical level, as attested by the values of 180.0 and 0.0° for τ and $\measuredangle$(Py,Ph), respectively. The comparison between the calculated values and those taken from the X-ray structure of *trans*-styrylpyridine[66] (presented in Table 1) shows that there is a very good agreement between the optimized and the experimental geometries. The small deviation from planarity that is observed in the experimental geometry ($\tau = 179.1°$) can be ascribed to packing effects, which are not present in our calculations performed for the molecule in the gas phase. The *cis* isomer is predicted to be markedly twisted, the expected values of τ and $\measuredangle$(Py,Ph) for a perfectly planar *cis* configuration being 0.0°. The non-planarity of this isomer can be ascribed to the steric hindrance between the neighboring *ortho* H substituents of the two cyclic rings. Note that there is no experimental structure for this isomer, which actually forms an oil.

The *trans*→*cis* isomerization gives rise to an increase of about 4° in the angles C^{Ph}–C^1–C^2 and C^1–C^2–C^{Py}, and is also accompanied by a lengthening (of about 0.01 Å) of the C^{Ph}–C^1 and C^2–C^{Py} bonds; this lengthening can be explained by the fact that these bonds lose much of their partial double-bond character. The nonplanarity of the structure of the *cis* isomer

prevents the delocalization of the π system over the whole molecule. The delocalization is therefore confined to the pyridinyl, phenyl, and C^1–C^2 moieties, for which no significant changes in the interatomic distances are observed (illustrated in Table 1 by the values reported for the C^1–C^2 bond length).

Table 3. Selected distances [Å] and angles [°] in optimized *trans* and *cis* geometries of 4-styrylpyridine (results of the calculations performed with the cc-pVDZ basis set).

	C^{Ph}–C^1	C^1–C^2	C^2–C^{Py}	C^{Ph}–C^1–C^2	C^1–C^2–C^{Py}	τ	$\measuredangle$(Py,Ph)
trans-4-styrylpyridine							
HF	1.478	1.331	1.478	126.6	125.7	178.3	35.2
MP2	1.471	1.361	1.470	125.5	125.1	177.2	38.9
B3LYP	1.467	1.351	1.466	127.2	126.4	180.0	0.0
PBE	1.465	1.361	1.464	127.3	126.4	180.0	0.0
cis-4-styrylpyridine							
HF	1.486	1.330	1.486	129.5	129.2	4.3	57.2
MP2	1.480	1.361	1.479	126.6	126.7	5.5	51.9
B3LYP	1.476	1.351	1.476	130.9	130.6	6.8	51.3
PBE	1.474	1.362	1.473	131.0	130.8	7.8	49.5

The *trans* conformation is expected to be the most stable isomer of 4-styrylpyridine, as its planar structure favors the delocalization of the π system over the whole molecule, and there is no steric hindrance between the substituents of the aromatic rings as in the case of the *cis* isomer. Consequently, the zero-point energy difference between the two isomers [Eq. (1)]:

$$\Delta E_{CT}^{\circ} = E^{\circ}(cis) - E^{\circ}(trans) \quad (1)$$

must be positive. The zero-point energy, E°, is the sum of the electronic (E^{el}) and the vibrational (E^{vib}) contributions. The former contribution is the energy minimum determined by geometry optimization, and the latter is that obtained from the vibrational analysis carried out on the optimized geometry within the harmonic approximation. Table 2 gives the calculated ΔE_{CT}° values as well as the corresponding electronic and vibrational contributions, ΔE_{CT}^{el} and ΔE_{CT}^{vib}, respectively.

Table 2. Calculated *cis*–*trans* zero-point energy differences, ΔE_{CT}° [cm^{-1}], and their electronic (ΔE_{CT}^{el}) and vibrational (ΔE_{CT}^{vib}) contributions [cm^{-1}].

	B3LYP		PBE	
	G	*G′*	*G*	*G′*
ΔE_{CT}^{el}	1690	1722	1629	1659
ΔE_{CT}^{vib}	51	−16	63	−35
ΔE_{CT}°	1741	1706	1692	1624

The ΔE_{CT}° values obtained with the B3LYP and PBE functionals are all positive and very consistent with each other. The *trans* isomer is therefore correctly predicted to be the most stable isomer. Furthermore, the zero-point energy difference is dominated by the electronic contribution, while the vibrational contribution is negligible [Eq. (2)]:

$$\Delta E_{CT}^{\circ} \approx \Delta E_{CT}^{el} \quad (2)$$

3.1.2. Wavefunction-Based Methods

Table 3 gives the values of selected distances and angles for the geometries obtained at the HF/cc-pVDZ and MP2/cc-pVDZ levels. For the two isomers, the comparison of the HF and MP2 data shows that the neglect of correlation in the HF calculations leads to C^{Ph}–C^1 and C^2–C^{Py} bonds that are $\approx$0.01 Å too long and to a C^1–C^2 bond that is too short by as much as $\approx$0.03 Å. These deviations also drastically affect the arrangement of the substituents of the C^1–C^2 photoisomerisable moiety, as attested by the large differences between the HF and MP2 values of the angular parameters. The comparison between the MP2 data and those obtained from the DFT calculations with the cc-pVDZ basis set and with the *G* and *G′* basis sets (Table 1) shows that the MP2 and DFT geometries are in reasonable agreement.

Surprisingly, the *trans* isomer is predicted to be planar by the DFT methods, while the HF and MP2 methods predict a slightly twisted structure. The latter studies yield τ and $\measuredangle$(Py,Ph) values that indeed deviate from the values of 180.0 and 0.0° expected for a planar geometry. Additionally, if the geometry optimization is carried out while constraining the symmetry to C_s, the HF and MP2 methods give a planar geometry that is (quasi) isoenergetic with the twisted geometry but corresponds to a saddle point characterized by a vibrational mode with an imaginary frequency. The instability along this mode can also be viewed as an instability along the twisting angular coordinate τ. The question as to whether the *trans* isomer is planar or not shows that a reliable description of the structural properties of 4-styrylpyridine is actually a challenging task. We now address this planarity issue, which proves to be a stringent criterion for comparing the performance of the different methods.

The DFT structures are very consistent with each other, and the discrepancies between these geometries and those obtained at the HF/cc-pVDZ level can be ascribed to a neglect of correlation. The discrepancies observed between the DFT and MP2 structures—especially for the *trans* isomer—may be caused by an insufficient dynamic-correlation recovery at the MP2/cc-pVDZ level. To probe this assumption, we determined the cross section of the S_0 ground-state PES along the angular coordinate τ in the vicinity of the planar configuration of the *trans* isomer at the MP2, CCSD, and CCSD(T) levels. To that end (with the HF, MP2, and CCSD energies being intermediate results in the CCSD(T) calculations), single-point studies at the CCSD(T)/cc-pVDZ level were carried out within the frozen-core approximation on the optimized B3LYP/*G′* *trans* geometry (τ =

180°) and on the B3LYP/G′ relaxed geometries obtained by varying τ (in steps of 1°) between 175 and 179°. These results are summarized in Figure 3.

The potential energy curves in Figure 3 are very flat, which shows that close to the most stable geometry of the *trans* isomer, the deformation along the angular coordinate τ corresponds to a floppy mode. In fact, for the two isomers of 4-styrylpyridine, the deformation along τ close to the minimum resembles that obtained by following the normal mode of lowest frequency, with the calculated B3LYP/G′ frequencies being 40 and 21 cm^{-1} for the *trans* and *cis* isomers, respectively. Within the accuracy of the grid used to scan the ground-state PES along τ, the potential energy curve obtained at the MP2/cc-pVDZ level clearly favors a slightly twisted geometry for the *trans* isomer. In contrast, the curves obtained at the more elaborate CCSD/cc-pVDZ and CCSD(T)/cc-pVDZ levels predict the planar structure to be the most stable one. These results support the idea that the deviation from planarity observed in the fully optimized MP2/cc-pVDZ geometry of *trans*-4-styrylpyridine is caused by an insufficient correlation recovery at this theoretical level (see also Section 3.1.3).

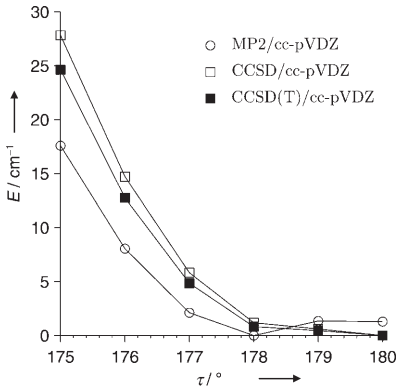

Figure 3. Cross section of the S_0 ground-state PES along the angular coordinate τ. The minima of the curves have been set to zero to ease their comparison (the lines serve as guides for eye).

Table 4 gives the HF/cc-pVDZ and MP2/cc-pVDZ zero-point energy differences and their electronic and vibrational contributions. The DFT values obtained for these quantities with the B3LYP and PBE functionals and the same cc-pVDZ basis set are also reported and are in very good agreement with those obtained with the *G* and *G*′ basis sets (Table 2). In all cases, the calculated *cis*–*trans* zero-point energy differences are positive, thus giving the *trans* isomer as the most stable one.

Table 4. Calculated *cis*–*trans* zero-point energy differences, ΔE_{CT}° [cm^{-1}], and their electronic (ΔE_{CT}^{el}) and vibrational (ΔE_{CT}^{vib}) contributions [cm^{-1}] (results of the calculations performed with the cc-pVDZ basis set).

	HF	MP2	B3LYP	PBE
ΔE_{CT}^{el}	1445	664	1888	1819
ΔE_{CT}^{vib}	26	21	−2	11
ΔE_{CT}°	1471	686	1885	1830

The HF ΔE_{CT}° value of 1471 cm^{-1} is surprisingly in good agreement with the DFT results, which indicates that the errors in the electronic energies of the isomers (caused by the neglect of correlation) compensate during the evaluation of ΔE_{CT}°. However, the MP2 value of 686 cm^{-1} corresponds to about one third of the DFT values. As compared to the DFT results, the underestimation of the stability of the *trans* isomer with respect to the *cis* isomer may be attributed to the insufficient recovery of correlation pointed out above. Using the optimized B3LYP/G′ geometries of the two isomers, we calculated (at the CCSD(T)/cc-pVDZ level) the electronic energy difference, ΔE_{CT}^{el}, which is shown by all the results to be the dominating contribution to ΔE_{CT}° [see Eq. (2)]. The values found with this basis set for ΔE_{CT}^{el} are 1520, 737, 901, and 873 cm^{-1} at the HF, MP2, CCSD, and CCSD(T) levels, respectively. The situation concerning the energetics improves on going from the MP2 to the CCSD(T) level, but there remains a factor of about two between the CCSD(T) value and those obtained with the DFT methods. The CCSD(T)/cc-pVDZ correlation energies of the *trans* and *cis* isomers are −2.005 and −2.008 Hartrees, respectively. Taking these values as the cc-pVDZ basis-set correlation energies of the two isomers, one finds for each isomer that the same amount of basis-set correlation energy (namely, 92.0 and 95.6%) is recovered at the MP2 and CCSD levels, respectively. The cc-pVDZ basis set is indubitably not flexible enough for correlated wavefunction-based methods, and we would have to use larger basis sets to improve our best ΔE_{CT}^{el} estimate of 873 cm^{-1}. This, however, is beyond the purpose of the present study.

In general, despite the observed discrepancies, it can be concluded that DFT and highly correlated wavefunction-based methods converge towards a similar description of the structural and energetic changes that accompany the *trans*⇄*cis* isomerization. Thus, on passing from the *trans* to the *cis* isomer, one goes from a planar geometry to a markedly twisted one (of higher energy), in which the C^{Ph}–C^{1} and C^{2}–C^{Py} bonds lose much of their partial double-bond character. The B3LYP hybrid and PBE GGA functionals perform equally well, and their use with a small basis set, such as the *G* basis set, already allows us to obtain very satisfactory results.

3.1.3. 4-Styrylpyridine versus Stilbene

The arrangements of the phenyl and pyridinyl fragments around the ethylenic moiety in the *cis* and *trans* ground-state geometries of 4-styrylpyridine are very similar, as attested by the identical lengths of the C^{Ph}–C^{1} and C^{2}–C^{Py} bonds and the very similar values found at all the studied theoretical levels for the C^{Ph}–C^{1}–C^{2} and C^{1}–C^{2}–C^{Py} angles (Tables 1 and 3). This similarity suggests that the two aromatic substituents, with their isoelectronic π systems, are nearly equivalent from the point of view of their interactions with the ethylenic moiety. If so, the ground-state conformational properties of 4-styrylpyridine should be very similar to those of stilbene (which has two equivalent phenyl substituents). This fact is effectively confirmed in Table 5. Thus, from the comparison of selected distances and angles in the optimized B3LYP/cc-pVDZ *cis* and

Table 5. Compared structures and energetics of the *trans* and *cis* isomers of 4-styrylpyridine and stilbene. Part A: Selected distances [Å] and angles [°] in optimized *cis* and *trans* geometries of 4-styrylpyridine (X = Py) and stilbene (X = Ph); Part B: *cis–trans* electronic energy differences, ΔE_{CT}^{el} [cm^{-1}], calculated for the two molecules at similar theoretical levels.

Part A	C^{Ph}–C^1	C^1–C^2	C^2–C^X	C^{Ph}–C^1–C^2	C^1–C^2–C^{Ph}	C^{Ph}–C^1–C^2–C^X
trans isomers (B3LYP/cc-pVDZ calculations)						
4-styrylpyridine[a]	1.467	1.351	1.466	127.2	126.4	180.0
stilbene[70]	1.468	1.351	1.468	127.1	127.1	180.0
trans isomers (MP2/aug-cc-pVDZ calculations)						
4-styrylpyridine[a]	1.470	1.364	1.469	126.2	125.5	180.0
stilbene[70]	1.471	1.364	1.471	126.2	126.2	180.0
cis isomers (B3LYP/cc-pVDZ calculations)						
4-styrylpyridine[a]	1.476	1.351	1.476	130.9	130.6	6.8
stilbene[70]	1.477	1.352	1.477	131.1	131.1	6.7

Part B ΔE_{CT}^{el}	MP2/cc-pVDZ	CCSD(T)/cc-pVDZ	B3LYP/cc-pVDZ
4-styrylpyridine[a]	664	873[b]	1888
stilbene[70]	670[c]	819[d]	1858

[a] This work. [b] CCSD(T)/cc-pVDZ single-point calculations on optimized B3LYP/*G′ cis* and *trans* geometries. [c] Results of geometry optimizations performed at the MP2/6-31G** level. [d] Estimates obtained from a focal-point analysis of the *cis–trans* energy difference performed on optimized B3LYP/cc-pVTZ *cis* and *trans* geometries.[70]

trans geometries of the two isolated molecules (see part A of Table 5), one can infer a close match between their geometries in either conformation. Furthermore, an inspection of part B of Table 5 shows that the *cis–trans* energy differences in isolated 4-styrylpyridine and isolated stilbene are identical within the accuracy of the ab initio methods employed.

For 4-styrylpyridine, which we characterized in vacuum and at 0 K, it still remains to definitively determine whether its geometry in the *trans* conformation is planar or not in the limit $T \rightarrow 0$ K. Indeed, as seen above, direct energy minimizations at the HF/cc-pVDZ and MP2/cc-pVDZ levels give nonplanar geometries, whereas strictly planar geometries are obtained with the DFT methods. The possibility of a planar geometry is also supported by the cross section determined at the CCSD(T)/cc-pVDZ level of the ground-state PES near the *trans* minimum. The analysis of the vibrational structures in the experimental electronic spectra of solvated *trans*-4-styrylpyridine[67] and solvated *trans*-stilbene[68] indicates that the geometries of both species are almost planar in glassy matrices and more or less nonplanar in fluid solutions. However, the analysis of the resolved rotational structure in the fluorescence spectrum of *trans*-stilbene—recorded on an ultra-cold (6 K), collision-free molecular beam—demonstrates that this species is strictly planar in vacuum and in its ground-state vibronic level.[69] Such an experiment has not been carried out so far for *trans*-4-styrylpyridine, but from the theoretical point of view,[70] it is known that the HF and MP2 methods give nonplanar geometries for *trans*-stilbene whereas the DFT methods give strictly planar geometries (which is in perfect agreement with experiment). Therefore, given the superior performance shown by the DFT methods, we can assert on the basis of our DFT results that *trans*-4-styrylpyridine is also strictly planar in vacuum and in the limit $T \rightarrow 0$ K.

Regarding the performance of correlated wavefunction-based methods for addressing this issue of planarity, Kwasniewski et al. showed in their study of *trans*-stilbene[70] that a correct description of the molecular structure actually requires the use of sufficiently flexible basis sets. In particular, using the relatively large aug-cc-pVDZ basis set, they could establish the planarity of *trans*-stilbene at the MP2 level for the first time. Furthermore, they observed a quite satisfactory agreement between the geometries they calculated at the MP2/aug-cc-pVDZ and B3LYP/aug-cc-pVDZ levels.[70]

We also optimized the geometry of *trans*-4-styrylpyridine at the MP2/aug-cc-pVDZ level by using the optimized nonplanar MP2/cc-pVDZ geometry as a starting point. The optimization led to a strictly planar geometry, whose selected distances and angles are reported in Table 5. These data compare quite well with those reported for the planar geometries obtained with the DFT methods (Tables 1 and 5), thus showing the good agreement between the involved geometries. Note also the similitude between the data reported in Table 5 for the calculated MP2/aug-cc-pVDZ structures of *trans*-stilbene and *trans*-4-styrylpyridine. Finally, regarding the use of wavefunction-based methods, it can be concluded that a sufficiently large and flexible basis set is required for achieving a reliable description of the structures of the two molecules.

Similarly, an accurate determination of the *cis–trans* energy differences in 4-styrylpyridine and stilbene with wavefunction-based procedures would actually require the use of a high-level method, such as CCSD(T), in combination with a sufficiently large basis set, such as aug-cc-pVDZ (or other even more flexible ones). However, this is currently impossible because of the large number of atoms in the molecules. Eliel and Engelsman recently proposed an up-to-date experimental estimate (of 1574–1749 cm^{-1}) for the *cis–trans* enthalpy difference, ΔH_{CT}°, of stilbene. The researchers derived this estimate from the heats of combustion of the two isomers in the gas phase.[71] By virtue of the equality between the *cis–trans* energy differences in the two molecules established at different theoretical levels (see Table 5), this value can be used as an estimate for the *cis–trans* enthalpy difference in 4-styrylpyridine as well. Neglecting the temperature dependence of the enthalpy of isomerization, (i.e. assuming the same temperature dependence for the enthalpies of both isomers), one has: $\Delta E_{CT}^{\circ} = \Delta H_{CT}^{\circ}$, that is, we propose the use of the same "experimental" estimate of the *cis–trans* zero-point energy difference (namely, 1574–1749 cm^{-1}) for both molecules; this estimate is

reproduced quite well by the DFT calculations (Tables 2, 4, and 5).

3.2. Reactivity of 4-Styrylpyridine in the Ground State

3.2.1. The Thermally Activated trans⇔cis *Isomerization*

Besides the photoinduced process,[72–74] the *trans*⇄*cis* isomerization of 4-styrylpyridine might also occur through a thermally activated process. This thermally activated pathway has not been observed so far. Still, a full characterization of the corresponding transition state, TS_0, based on first-principles methods is possible. It can be anticipated on chemical grounds that the geometry of 4-styrylpyridine at such a transition state is markedly rotated, with a twist angle τ of about 90°. Consequently, we first searched for saddle points on the S_0 surface by carrying out restricted calculations at the PBE/*G* and B3LYP/*G* levels (starting from relaxed geometries obtained for fixed τ values between 80 and 100°). None of these calculations allowed the sought transition state to be located. Instead, three other extrema were obtained, and frequency analysis allowed us to identify them as first-order saddle points; they correspond to internal rearrangements close to the *cis* and *trans* minima and will be discussed later on.

The inspection of the starting geometries helped us to understand why these calculations ended near those minima. It turns out that if the starting geometries are obtained from the geometry of the *trans* (or *cis*) isomer, the conformation of the substituents in these partially relaxed geometries remains *trans* (or *cis*). The same observations were made by Han et al.[75] when dealing with the construction of the ground-state potential energy curve of stilbene along the twisting angular coordinate defined by the torsion angle C^{Ph}–C^1–C^2–C^{Ph}, which relates the two phenyl substituents. In the geometries that they obtained by varying C^{Ph}–C^1–C^2–C^{Ph}, the substituents H^1 and H^2 remained *cis* or *trans* to each other depending on whether the starting geometry was that of the *cis* isomer or that of the *trans* isomer. They solved the problem by constraining the angles C^{Ph}–C^1–C^2–C^{Ph} and H^1–C^1–C^2–H^2 to be equal while rotating the ethylenic C=C bond.[75] Similarly, the starting geometry used in our search of TS_0 was determined by optimizing the molecular structure of 4-styrylpyridine while constraining $\theta_C = C^{Ph}$–C^1–C^2–C^{Py} and $\theta_H = H^1$–C^1–C^2–H^2 to 90°. However, the different restricted calculations carried out with this starting geometry remain inconclusive.

This probably follows from the fact that 4-styrylpyridine actually acquires a significant biradical character (in the same way the parent stilbene molecule does)[75] upon breakage of the ethylenic π bond, that is, 4-styrylpyridine (at TS_0) can be better viewed as an open-shell singlet (OSS) biradical, L$^{\bullet}$–$^{\bullet}$R, where L and R refer to the [PhH^1C^1] and [C^2H^2Py] moieties, respectively. Hence, the difficulties met can be ascribed to the fact that the electronic structure of biradicals[76–78] corresponds to a situation of strong static correlation, which cannot be handled correctly within the restricted single-determinantal Kohn–Sham (KS) framework with the available approximate functionals.[79–83] This effect also manifests itself by the instability of the restricted KS wavefunction. Indeed, unrestricted single-point calculations performed with the PBE and B3LYP functionals on the starting geometry led to solutions that are lower in energy than those obtained by restricted calculations carried out under the same conditions.

An accurate description of OSS biradicals within the restricted single-determinantal KS framework requires functionals that fully include left–right correlation, which, of course, is the case for the exact exchange–correlation functional. The self-interaction error of approximate functionals mimics left–right correlation effects,[84–89] but it does so in an unspecified manner, and the strong static correlation in OSS biradicals remains underestimated in the restricted single-determinantal DFT approach; this leads to solutions that are too high in energy. Optimized geometries are also erroneous,[81] and this probably explains why we have not been able to locate the transition state TS_0 in that way. Filatov and Shaik[80] recently developed the "spin-restricted ensemble-referenced KS" (REKS) method, within which conventional approximate functionals can be used to efficiently cope with such a situation of strong static correlation. In this scheme, the ground-state density is given by a symmetry-adapted weighted sum of single-determinantal densities while the energy is given by a corresponding weighted sum of single-determinantal energies.[80] The REKS method enables one to tackle the electronic-structure problem within the desired spin and spatial symmetry, in contrast to the unrestricted DFT approach to which we have resorted. Unrestricted DFT helps overcome the deficiency of the approximate functionals in that static correlation effects are included thanks to the flexibility of the wavefunction. Indeed, given that the spatial parts of spin-up (α) and spin-down (β) molecular orbitals (MOs) are allowed to differ, the single electrons of the biradicals occupy two distinct orbitals, α-HOMO and β-HOMO (HOMO = highest occupied MO), centered on different parts of the molecule, and can thus avoid each other in an efficient way (for 4-styrylpyridine at TS_0, see Figure 4).

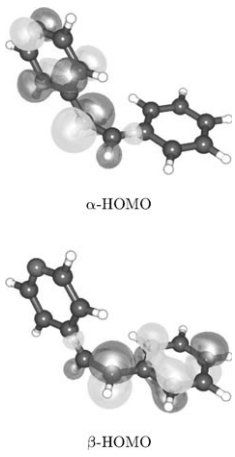

Figure 4. Highest occupied α and β MOs obtained from unrestricted B3LYP/*G* calculations for 4-styrylpyridine at TS_0 (which has the structure of an OSS biradical). These orbitals are π-type orbitals localized on the [PyH^2C^2] and [C^1H^1Ph] fragments; they are occupied by the single electrons, which are kept distant from each other.

As recently reviewed by Gräfenstein et al.,[82] unrestricted DFT can perform quite well for the geometry and the energy of OSS biradicals, such as rotated alkenes. This performance is, however, at the expense of artificially breaking the spin symmetry of the molecule and possibly also its spatial symmetry (if any). The broken-symmetry (BS) KS determinant is not a spin-symmetry-adapted wavefunction, as it is a mixture of a singlet and ($M_S = 0$) triplet functions. To account for the importance of the triplet contribution, the energy of the biradical singlet state E_S is evalu-

ated according to Equation (3):[79]

$$E_S = E_{BS} + (E_T - E_{BS}) \times \frac{\left\langle \hat{S}^2 \right\rangle_S - \left\langle \hat{S}^2 \right\rangle_{BS}}{\left\langle \hat{S}^2 \right\rangle_T - \left\langle \hat{S}^2 \right\rangle_{BS}} \quad (3)$$

where E_{BS} is the energy of the BS state, E_T is the energy of the triplet state at the same geometry, and $\hat{S}$ is the total electronic spin operator. The expectation values $\left\langle \hat{S}^2 \right\rangle$ are evaluated using the appropriate KS wavefunctions. Equation (3) evidences the fact that the BS results are most reliable when the singlet–triplet energy difference is small[79] or that the spin contamination of the BS wavefunction vanishes.

The unrestricted optimization calculations carried out at the PBE/*G* and B3LYP/*G* levels finally allowed the determination of the TS_0 state. As shown by the selected distances and angles reported in Table 6, the geometries obtained with the two functionals are very similar. The optimized B3LYP/*G* geometry is represented in Figure 4 along with the localized α-HOMO and β-HOMO orbitals, which are centered on the [PyH^2C^2] and [C^1H^1Py] fragments, respectively. These two frontier MOs are very similar, which stresses once more that the two aromatic rings are quasi-equivalent from the point of view of their interactions with the ethylenic group. Frequency calculations gave one imaginary frequency, thus showing that the characterized extremum corresponds to a first-order saddle point.

Table 6. Structural parameters [Å, °] and barrier height, $\Delta E_0^{\neq}$ [cm^{-1}], characterizing the biradical transition state TS_0 associated with the *trans*⇄*cis* isomerization of 4-styrylpyridine (X = Py).[a]

	4-styrylpyridine		stilbene[b]
	B3LYP/*G*[c]	PBE/*G*[c]	ref. [75][d]
C^{Ph}–C^1	1.421	1.424	1.420
C^1–C^2	1.470	1.468	1.464
C^2–C^X	1.424	1.426	1.420
C^{Ph}–C^1–C^2	125.4	125.2	125.6
C^1–C^2–C^X	125.3	125.2	125.6
$\theta_C = C^{Ph}$–C^1–C^2–C^X	91.9	91.7	90.2
$\theta_H = H^1$–C^1–C^2–H^2	86.3	86.5	88.5
τ	88.3	88.1	–
$\Delta E_0^{\neq}$[e]	15720	15914	15704

[a] The barrier height is taken relative to the energy of the most stable *trans* isomer. [b] This column helps compare our results with those obtained for stilbene (X = Ph) at the biradical transition state associated with the *trans*⇄*cis* isomerization. [c] This work. [d] Results of broken-symmetry calculations performed with the B88P86 GGA functional and a Slater-type orbital basis set of valence triple-ζ polarized quality.[75] [e] Not corrected from the zero-point vibrational contribution.

Taking the energy of the *trans* isomer as the zero of energy, the BS state is found to lie at 15880 and 16012 cm^{-1} at the B3LYP/*G* and PBE/*G* levels, respectively. In both cases, the quantity $E_T - E_{BS}$ proves to be small, namely, 150 and 95 cm^{-1}. Taking the respective values of 1.057 and 2.052 for $\left\langle \hat{S}^2 \right\rangle_{BS}$ and $\left\langle \hat{S}^2 \right\rangle_T$ at the B3LYP/*G* level, and of 1.025 and 2.021 for the two quantities at the PBE/*G* level, we calculated E_S values of 15720 and 15914 cm^{-1} by using Equation (3) (see Table 6). This result gives quite small B3LYP and PBE values for the singlet–triplet splitting at TS_0 (i.e. 309 and 192 cm^{-1}, respectively), which makes us confident about the quality of our BS results. Recalling that E_S actually corresponds to the barrier height $\Delta E_0^{\neq}$ for the isomerization reaction, it turns out that the B3LYP and PBE functionals perform similarly for the description of the isomerization of 4-styrylpyridine.

Using the BS-DFT method, and including spin projection [see Eq. (3)], Han et al. obtained a barrier height of $\Delta E_0^{\neq} = 15704$ cm^{-1} for the isomerization of stilbene, which is in good agreement with the experimental estimate of 15039–18817 cm^{-1} (see ref. [75] and references therein). This value compares quite well with our values for 4-styrylpyridine. Furthermore, the comparison of the structural data reported in Table 6 also shows that the geometries of the two molecules at the transition states are very close. Hence, one can draw the conclusion that the thermally activated *cis*⇄*trans* isomerization reaction pathways of stilbene and 4-styrylpyridine are very similar. Figure 5 shows the ground-state potential energy curve of 4-styrylpyridine along the twist angle θ_C.

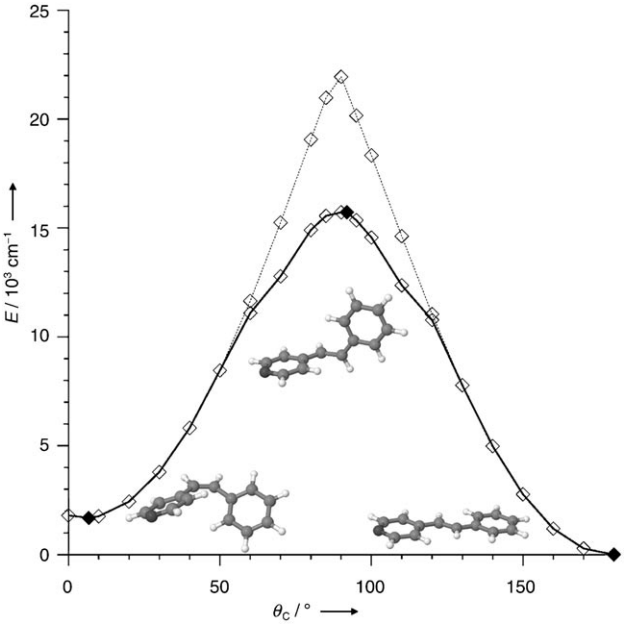

Figure 5. Ground-state potential energy curve of 4-styrylpyridine along the torsion-angle coordinate θ_C; results of restricted (light dashed line) and BS (bold solid line) calculations at the B3LYP/*G* level. The open symbols represent the results of partial optimizations, performed with fixed values of $\theta_C = \theta_H$, while the filled symbols represent the full optimizations carried out for characterizing the minima associated with the *cis* and *trans* isomers and the TS_0 transition state. The energy of the *trans* conformer is taken as the zero of energy. An instability of the restricted KS solution is observed for θ_C values between 50 and 130°.

3.2.2. *Specific Reactivity of the* cis *and* trans *Isomers*

As previously indicated, the very first restricted KS calculations that were carried out allowed the identification of three first-order saddle points on the S_0 surface, namely, the transition states TS_i ($i = 1,2,3$; Figure 6).

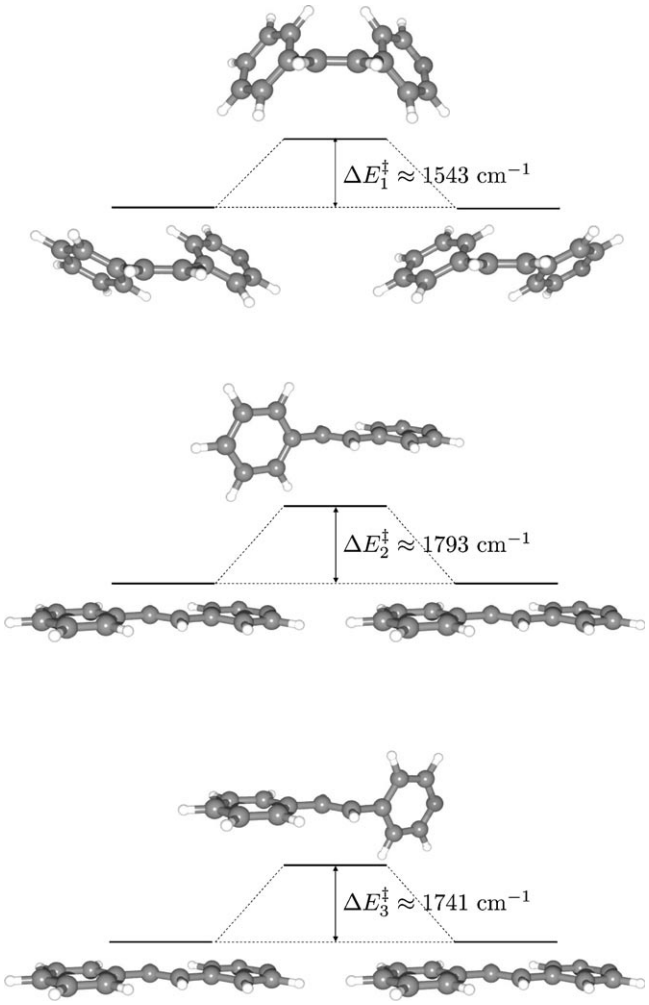

Figure 6. Energy profiles of the enantiomerization of *cis*-4-styrylpyridine (top) and of the rotation of the phenyl group (middle) and the rotation of the pyridinyl group (bottom) in *trans*-4-styrylpyridine. The geometries shown for the transition states and the isomers were obtained at the B3LYP/*G* level. The values of the barrier heights correspond to the averaged B3LYP/*G* and PBE/*G* values.

Table 7. Barrier heights, $\Delta E_i^{\ddagger}$ [cm^{-1}], for the enantiomerization in the *cis* isomer ($i=1$) and the rotation of the phenyl ($i=2$) and the pyridinyl group ($i=3$) in the *trans* isomer of 4-styrylpyridine (see Figure 6). Selected distances [Å] and angles [°] characterizing the transition states are also given.

	$\Delta E_i^{\ddagger}$ [a]	C^{Ph}–C^1	C^1–C^2	C^2–C^{Py}	C^{Ph}–C^1–C^2	C^1–C^2–C^{Py}	τ	∢(Py,Ph)
TS_1: enantiomerization of *cis*-4-styrylpyridine								
B3LYP/*G*	1479	1.485	1.348	1.485	130.4	130.1	0.5	80.1
PBE/*G*	1607	1.480	1.361	1.480	132.0	131.6	0.5	71.8
TS_2: rotation of the phenyl group in *trans*-4-styrylpyridine								
B3LYP/*G*	1703	1.492	1.345	1.474	123.8	126.9	180.0	89.7
PBE/*G*	1883	1.491	1.354	1.472	123.7	126.9	180.0	89.9
TS_3: rotation of the pyridinyl group in *trans*-4-styrylpyridine								
B3LYP/*G*	1646	1.474	1.345	1.491	127.6	123.6	180.0	89.8
PBE/*G*	1836	1.473	1.355	1.490	127.6	123.5	180.0	90.0

[a] Not corrected from the zero-point vibrational contribution.

TS_1 is the transition state associated with the interconversion of the Λ and Δ enantiomers of *cis*-4-styrylpyridine, whose chirality stems from the fact that it is a helicenoid diarylethene. As shown in Table 7, the B3LYP and PBE functionals consistently give values of 1607 and 1479 cm^{-1}, respectively, for the barrier height of this reaction, from which one deduces $\Delta E_1^{\ddagger} \approx 1543\ cm^{-1}$.[90] The structural parameters given in Table 7 show that the structures obtained at the B3LYP/*G* and PBE/*G* levels are relatively similar. The geometry of 4-styrylpyridine at TS_1 is thus characterized by the fact that the four atoms C^{Ph}, H^1, H^2, and C^{Py} are nearly located in the same plane ($\tau = 0.5°$), while the angle between this plane and that of the phenyl or pyridinyl ring is ≈50° (or ≈57°), according to the B3LYP/*G* (or PBE/*G*) results. This value is somewhat larger than that of ≈37° (or ≈35°) found for the geometry of the *cis* isomer. It follows that the delocalization over the whole molecule is more pronounced in the *cis* configuration than in the configuration at TS_1. This effect is attested by the lengthening (by ≈0.007 Å) of the C^{Ph}–C^1 and C^2–C^{Py} bonds on going from the former geometry to the latter, which follows from the decrease of their partial double-bond character.

For the geometry at TS_1, Table 7 shows a difference of ≈1.5° between the B3LYP/*G* and PBE/*G* values of the C^1–C^2–C^{Py} and C^{Ph}–C^1–C^2 angles and a larger difference (of about 8°) between the values found for the angle ∢(Py,Ph) at the two theoretical levels. Consequently, the two functionals do not predict the same arrangement of the two cyclic rings, which actually tend to be oriented face to face. This orientation is favorable to π interactions, and the differences observed can be ascribed to the fact that an accurate DFT characterization of such weak, long-range interactions remains a challenging task.[91] However, it is worth noting that in either of the calculated geometries, the two aromatic substituents adopt a comparable arrangement around the ethylenic moiety.

On the other hand, the B3LYP and PBE functionals give very similar results for the geometries at the transition states TS_2 and TS_3, which are associated with the rotation of the phenyl and pyridinyl groups, respectively, in *trans*-4-styrylpyridine. The two geometries are very similar. In both cases, the plane of the rotating group is perpendicular to the plane defined by the rest of the molecule. Because of the vanishing interaction between the π systems of the two moieties, the bonds that connect them are ≈0.024 Å longer than in the *trans* geometry (Table 1). As compared to the *trans* geometry, the structure at TS_2 (or TS_3) exhibits a shortening (of about 0.006 Å) of the C^1–C^2 bond and an identical lengthening of the C^{Ph}–C^1 (or C^2–C^{Py}) bond. For either of the structures at the TS_2 and TS_3 transition states, this increased bond-length alternation probably reflects the antiaromaticity of the largest fragment, whose π system contains $8 = 4 \times 2$ electrons.

Inspection of Table 7 shows that the B3LYP and PBE functionals perform quite similarly, also for the energetics of these

internal rotations. Indeed, although the values obtained with the PBE functional for $\Delta E_2^{\neq}$ and $\Delta E_3^{\neq}$ are systematically $\approx 180\ cm^{-1}$ larger than those obtained with the B3LYP functional, this difference remains well below the chemical accuracy of 350 cm^{-1} ($\approx 1\ kcal\ mol^{-1}$). Most importantly, whatever the theoretical level, it is true that $\Delta E_2^{\neq} \approx \Delta E_3^{\neq}$. This result, in conjunction with the similarities between the geometries at TS_2 and TS_3 (and the similar arrangements of the phenyl and pyridinyl substituents in the geometry at TS_1), reflects the near equivalence of the two aromatic rings with regard to their interactions with the ethylenic group, which we already pointed out (see Section 3.1.3).

The rotation of one phenyl ring in *trans*-stilbene was characterized by Kwasniewski et al. at the B3LYP/cc-pVTZ level.[70] The geometry of stilbene at the transition state is very similar to that of 4-styrylpyridine at TS_2 or TS_3, and the barrier height of 1679 cm^{-1} compares very well with the values found for $\Delta E_2^{\neq}$ and $\Delta E_3^{\neq}$ at the B3LYP/*G* level (which average to 1675 cm^{-1}). This similitude adds to the other strong resemblances which we have evidenced so far for isolated stilbene and 4-styrylpyridine in their ground state. On their basis, it can be anticipated that the cross sections of the ground-state PESs of the two isolated molecules along relevant common configurational coordinates are superimposable in a close to quantitative manner. The relevant coordinates are those reaction coordinates that describe the individual and concerted torsional motions of the aromatic substituents around the photoisomerisable ethylenic moiety.

3.3. Temperature Effect on the Geometries of the *cis* and *trans* Isomers

Thermal fluctuations are known to affect significantly the absorption and fluorescence spectra of solvated *trans*-4-styrylpyridine,[67] which exhibit a blurring of the vibronic structure and an hypsochromic shift on passing from cryogenic to room temperatures. This has been explained by the transition from an almost planar structure in glassy matrices to more or less nonplanar forms in fluid solutions. The cause for this effect is a twisting about the quasi-single C^{Ph}–C^1 and C^2–C^{Py} bonds.[67] In the following, we will examine the influence of temperature on the *cis* and *trans* ground-state geometries of the isolated molecule through Car–Parrinello MD calculations at the PBE/*P* level.

As shown in Table 1, the calculation conditions used herein give optimized *cis* and *trans* geometries that are in very good agreement with those obtained at the PBE/*G*′ level. This also holds for the calculated *cis*–*trans* energy difference, ΔE_{CT}^{el}, which amounts to 1806 cm^{-1}, as compared to the PBE/*G*′ value of 1624 cm^{-1}. This makes us quite confident about the quality of the MD calculations. The simulations carried out for ≈ 2.4 ps at target temperatures of 50, 150, and 300 K resulted in average ionic temperatures of 50 ± 8, 150 ± 24, and 295 ± 44 K for the runs with the *cis* isomer, and of 49 ± 6, 150 ± 23, and 302 ± 41 K for those with the *trans* isomer. For each simulation, the atomic positions were recorded every 40 a.u. (≈ 0.968 fs). At all temperatures, the geometry of each isomer exhibited significant fluctuations (whose amplitudes increased with temperature). This is illustrated by the plots of the time evolutions of the C^1–C^2 ethylenic bond length and of the angles $\theta_C = C^{Ph}$–C^1–C^2–C^{Py} and $\theta_H = H^1$–C^1–C^2–H^2 (Figure 7). The average values and the standard deviations found for these structural parameters are given in Table 8, along with the values found for these parameters in the optimized geometries.

Table 8. Results of the CPMD simulations: Average values and standard deviations found for the structural parameters C^1–C^2 [Å], $\theta_C = C^{Ph}$–C^1–C^2–C^{Py} [°], and $\theta_H = H^1$–C^1–C^2–H^2 [°].[a]

	Optim.	CPMD					
		50 K		150 K		300 K	
		Av.	Std. dev.	Av.	Std. dev.	Av.	Std. dev.
trans-4-styrylpyridine							
C^1–C^2	1.350	1.353	0.010	1.354	0.017	1.355	0.023
θ_C	180.0	178.7	2.7	179.8	6.3	178.2	8.4
θ_H	180.0	180.3	4.1	181.7	5.4	180.4	9.0
cis-4-styrylpyridine							
C^1–C^2	1.350	1.353	0.010	1.354	0.019	1.357	0.025
θ_C	7.7	8.0	4.0	−2.4 (−7.1)	9.2 (6.7)	6.0	10.8
θ_H	5.2	5.1	3.0	−1.7 (−4.8)	7.6 (6.8)	4.6	9.2

[a] The statistics were performed on the data collected during ≈ 2.4 ps of simulation. In the case of the *cis* isomer, the values given in parentheses for the simulation carried out at 150 K were obtained from the analysis performed on the data collected during the last picosecond of the run. The values found in the optimized *cis* and *trans* geometries are also reported for comparison.

The inspection of Table 8 and Figure 7 shows that, with the exception of θ_C and θ_H for the simulation performed at 150 K on the *cis* isomer, the parameters rapidly vary around their average values, which do not significantly evolve with the temperature and stay quite close to those found in the optimized geometries. One also notes that the average amplitudes of the variations, as measured by the standard deviations, significantly increase with the temperature. In the case of the simulation run at 150 K on the *cis* isomer, the statistics performed on the values of θ_C and θ_H—collected during the whole simulation time of ≈ 2.4 ps—lead to negative averages (Table 8). This can be explained by the fact that the rotation of the pyridinyl ring about the C^2–C^{Py} bond occurs between ≈ 0.3 and ≈ 1.4 ps and translates into the enantiomerization of the *cis* isomer. The reaction that takes place can be better apprehended by considering the time evolutions shown in Figure 8 for the angles $\phi_{Ph} = C^2$–C^1–C^{Ph}–$C^{o\text{-}Ph}$ and $\phi_{Py} = C^1$–C^2–C^{Py}–$C^{o\text{-}Py}$ (see Figure 1 for the atom labeling), which precisely measure the twisting of the aromatic rings about the C^{Ph}–C^1 and C^2–C^{Py} bonds, respectively.

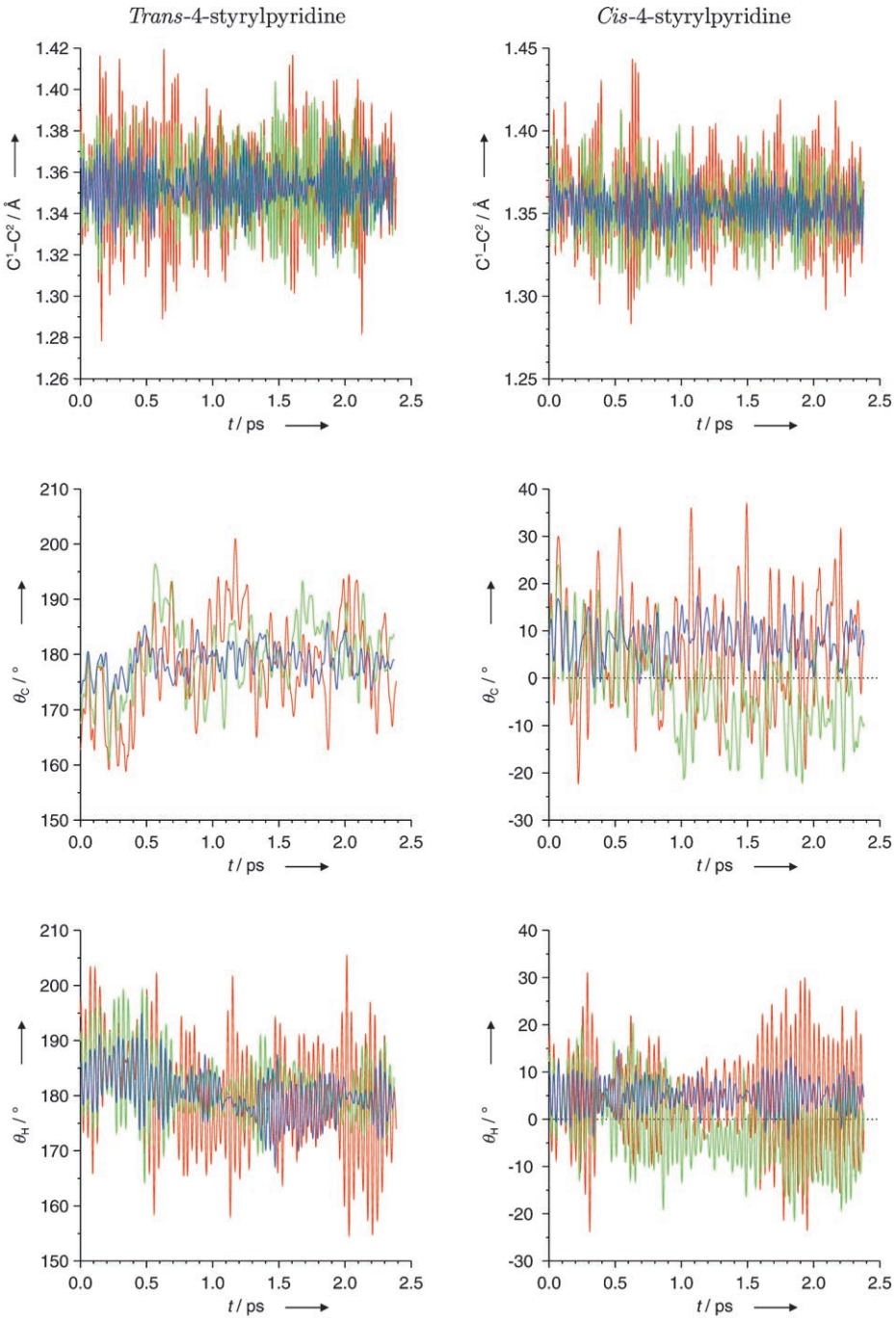

Figure 7. Time evolutions of the C^1–C^2, θ_C, and θ_H structural parameters, as deduced from the CPMD simulations performed at 50 K (blue line), 150 K (green line), and 300 K (red line) on the *cis* and *trans* isomers.

During the first ≈0.3 ps of simulation, the values of ϕ_{Ph} and ϕ_{Py} differ from those found in the optimized *cis* geometry of Δ configurations (namely, $\phi_{Ph}=34.4^\circ$ and $\phi_{Py}=34.2^\circ$), although still staying relatively close to them. Thereafter, the pyridinyl ring starts to rotate, which is attested by the strong increase of ϕ_{Py}. Concomitantly, the rotation of the phenyl ring takes place and gives rise to the observed decrease of ϕ_{Ph}. At ≈0.8 ps, the system is in the vicinity of the transition state, which is characterized by $\phi_{Py}=90.0^\circ$ and $\phi_{Ph}=0.0^\circ$ (see below). At ≈1.4 ps, the rotation of the phenyl ring is completed. The remainder of the simulation deals with the evolution of the product, which is the Λ enantiomer, as shown by the values recorded during the last picosecond of the simulation for ϕ_{Ph} and ϕ_{Py} (Figure 8) and for θ_C and θ_H (Figure 7 and Table 8). Indeed, in the optimized geometry of the Λ enantiomer, $\phi_{Ph}=-34.4^\circ$, $\phi_{Py}=-34.2^\circ$, or equivalently, $\phi_{Py}=145.8^\circ$, $\theta_C=-7.2^\circ$, and $\theta_H=-5.2^\circ$. Figure 9 shows snapshots taken from this run.

In unconstrained ab initio MD simulations started with one minimum, as in our case, a switch to another minimum is rarely observed within the computationally affordable simulation time. The direct observation of the rotation of the pyridinyl ring during the ≈2.4 ps of simulation performed on the *cis* isomer at 150 K is therefore fortuitous and results from very favorable conditions. We have characterized the transition state (TS_4) associated with this rotation and also the transition state associated with the rotation of the phenyl ring (TS_5). The calculations were done at the B3LYP/*G* and PBE/*G* levels. The results obtained with the two functionals are very consistent and are summarized in Figure 10 and Table 9. In line with the previously noticed quasi-equivalence of the two aromatic rings, the two transition states are structurally and energetically very close. The arrangements of the substituents around the ethylenic group simply interchange on passing from one transition-state structure to the other (Table 9). In particular, the rotating fragment is, in both cases, perpendicular to the plane defined by the rest of the molecule; the molecular symmetry is C_S. The coplanarity of the nonrotating ring and the ethylenic fragment is favorable to π interactions, which may help to stabilize the transitions states. This fact and the decreased strength of the C^{Ph}–C^1 and C^2–C^{Py} bonds on going from the *trans* to the *cis* isomer may probably converge to give the small rotation barriers found for the *cis* isomer. Indeed, the heights of the rotation barriers of the pyridinyl and phenyl groups are $\Delta E_4^{\ddagger}$

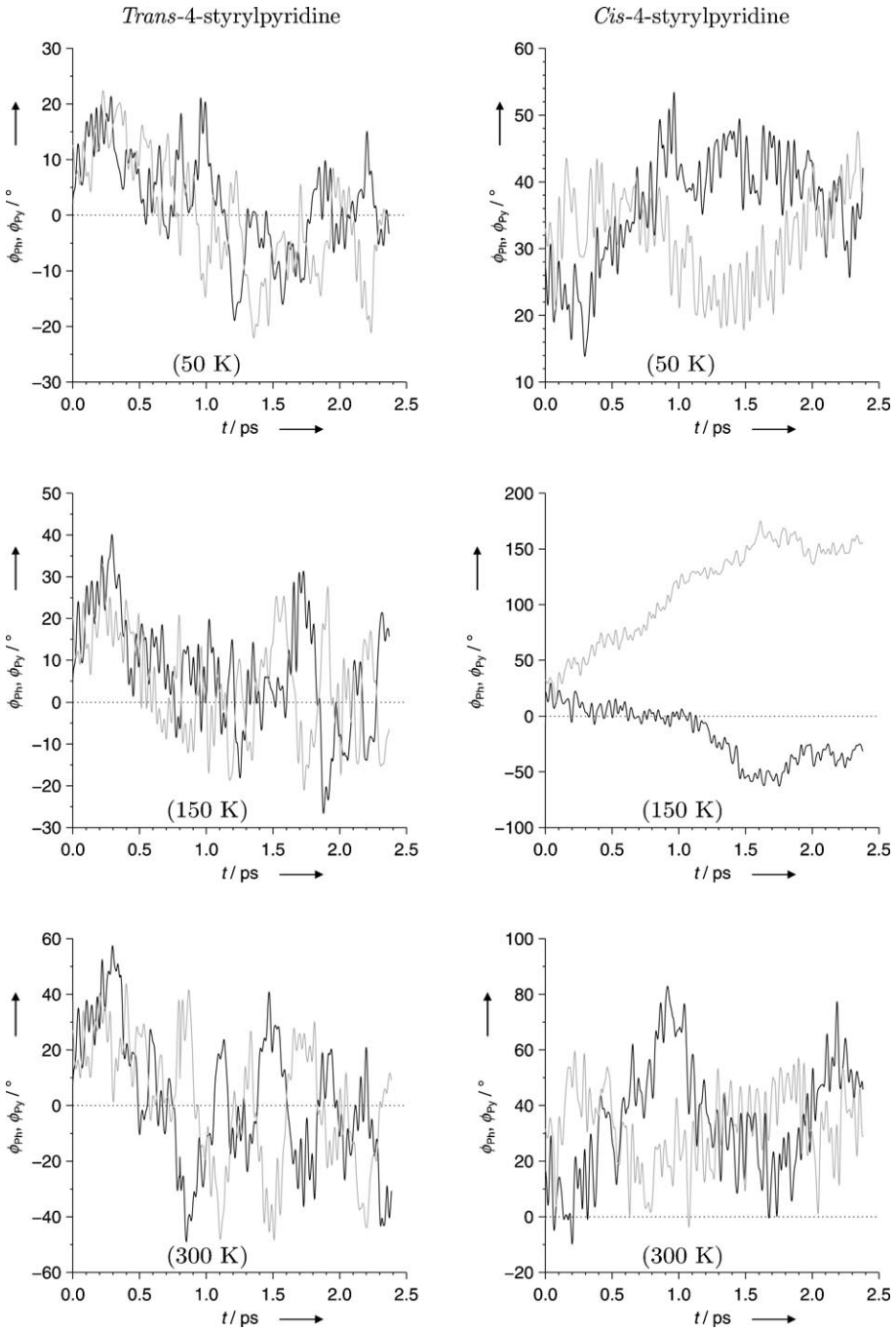

Figure 8. Time evolutions of the torsion angles, ϕ_{Ph} (black line) and ϕ_{Py} (gray line), as deduced from the CPMD simulations performed at 50, 150, and 300 K on the *cis* and *trans* isomers.

$\approx 588\ cm^{-1}$ and $\Delta E_5^{\neq} \approx 583\ cm^{-1}$, respectively, as obtained by averaging the PBE and B3LYP values (Table 9). These values are about three time smaller than those found for the *trans* isomer (Table 7). Hence, the rotation of the aromatic substituents is expected to take place far more readily in the *cis* isomer than in the *trans* isomer. Incidentally, in the MD simulation performed at 150 K on the *cis* isomer, the rotation of the pyridinyl ring was observed to occur completely within ≈ 1 ps.

Outside the timeslot in which the reaction takes place, the time evolutions of the torsion angles ϕ_{Ph} and ϕ_{Py} exhibit high-frequency fluctuations, which do not mask the fact that the variations of these parameters are principally characterized by large departures from their optimized values of $|\phi_{Ph}| = 34.4°$ and $|\phi_{Py}| = 34.2°$ for long periods of several tenths of a picosecond. These observations extend to the variations of ϕ_{Ph} and ϕ_{Py} in the simulations performed at 50 and 300 K on the *cis* isomer as well as in all those carried out on the *trans* isomer (in the optimized geometry of the *trans* isomer, $\phi_{Ph} = \phi_{Py} = 0.0°$). For both isomers, the amplitudes of the variations of ϕ_{Ph} and ϕ_{Py} are actually increasing functions of the temperature (see Figure 8). The relatively large amplitudes of these variations show that in the vicinity of the *cis* and *trans* minima, the ground-state PES is very flat along the ϕ_{Ph} and ϕ_{Py} angular coordinates. Remarkably, for both isomers—and whatever the temperature—the instantaneous evolutions of ϕ_{Ph} and ϕ_{Py} tend to take place in opposite directions, that is, from the point of view of an observer sitting on the ethylenic bond, the phenyl and pyridinyl rings undergo concerted clockwise–counterclockwise rotations about the C^{Ph}–C^1 and C^2–C^{Py} bonds. Finally, regarding the issue of planarity of the structure of the *trans* isomer, our simulations show that this species mainly exists in a nonplanar form at finite temperatures, the deviation from planarity being an increasing function of the temperature. Similarly, the *cis* isomer essentially adopts, at finite temperatures, twisted forms, whose departures from the optimized *cis* geometry increase with increasing temperature. These results are also valid for 4-styrylpyridine in condensed media, except that the environment probably reduces the extent to which the aromatic substituents can rotate. For the isolated molecule, the influence of the thermal fluctuations on the absorption spectra of its two isomers is being investigated, and the results will be reported elsewhere.

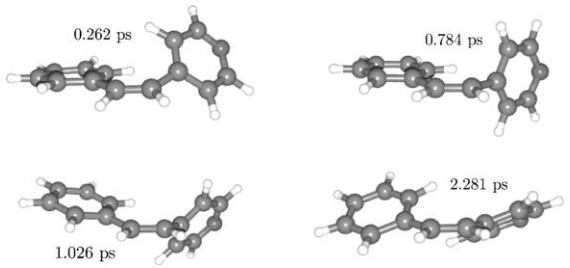

Figure 9. Snapshots taken from the simulation performed on the *cis* isomer at 150 K (see text). At 0.262 ps, the isomer has a Δ configuration. At 0.784 ps, the molecule is in the vicinity of the transition state associated with the rotation of the pyridinyl ring and its configuration is undetermined. The snapshots taken at 1.026 and 2.281 ps show that the molecule adopts a Λ configuration upon completion of the rotation of the pyridinyl ring.

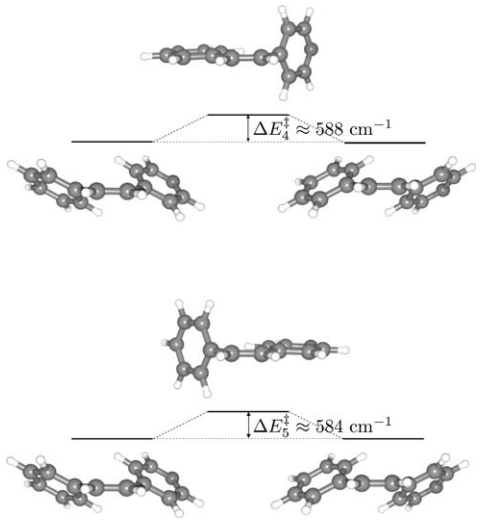

Figure 10. Energy profiles of the rotation of the pyridinyl (top) and phenyl (bottom) groups in *cis*-4-styrylpyridine. The geometries shown for the transition states and the isomers were obtained at the B3LYP/*G* level. The values of the barrier heights correspond to the averaged B3LYP/*G* and PBE/*G* values.

4. Conclusions

We characterized 4-styrylpyridine at different stationary points of its ground-state PES within DFT. The calculations were carried out with the PBE GGA and the B3LYP hybrid functionals, which were used in combination with basis sets of different qualities. For the geometries and relative stabilities of the *trans* and *cis* isomers, we obtained results that were remarkably consistent and that allowed us to draw the following conclusions: The molecular structure is strictly planar at the minimum associated with the *trans* conformation and becomes markedly twisted on passing to the minimum associated with the *cis* conformation. The calculations carried out with the two functionals and the DFT basis sets *G* and *G*′ gave values for the *cis*–*trans* zero-point energy difference that varied between 1624 and 1741 cm^{-1}. These values were spread over a quite narrow interval, and their midpoint provided a very good theoretical estimate of the zero-point energy difference, that is, $\Delta E_{CT}^{\circ} \approx 1680\ cm^{-1}$ ($\Delta E_{CT}^{\circ} \approx 4.8\ kcal\,mol^{-1}$).

Post-HF methods were also used to investigate the geometries and relative stabilities of the two isomers. The cc-pVDZ basis set was employed for these studies, and the calculations with the PBE and B3LYP functionals were re-conducted with this basis set to allow a rigorous comparison between the different methods. The DFT results thus obtained were in very good agreement with the other DFT results, but the flexibility of the cc-pVDZ basis set proved to be insufficient to allow a reliable characterization of 4-styrylpyridine at the MP2 level (or at even higher ones). In particular, MP2/cc-pVDZ calculations led to the prediction of a nonplanar geometry for the *trans* isomer and to a ΔE_{CT}° value of 686 cm^{-1}, which is about one third of the DFT values. By increasing the level of the treatment of the electronic correlation up to the CCSD(T) level, the discrepancy between the DFT and post-HF results was shown to decrease. It was thus possible to deduce the planarity of the geometry of the *trans* isomer from the cross section of the ground-state PES performed in the vicinity of the *trans* minimum and along the τ angular coordinate by means of CCSD(T)/cc-pVDZ calculations on B3LYP/*G*′ optimized geometries. Similarly, CCSD(T)/cc-pVDZ calculations on the B3LYP/*G*′ optimized *cis* and *trans* geometries gave a value of 873 cm^{-1} for ΔE_{CT}^{el} (which is the dominating electronic contribution to ΔE_{CT}°, i.e. $\Delta E_{CT}^{\circ} \approx \Delta E_{CT}^{el}$). The calculated *cis*–*trans* energy difference thus increases on going from the MP2/cc-pVDZ level to the CCSD(T)/cc-pVDZ level, but a factor of about two still remains between this value and the DFT best estimate of 1680 cm^{-1}.

It actually turned out to be necessary to resort to the larger aug-cc-pVDZ basis set to obtain a fully optimized planar geometry of the *trans* isomer at the MP2 level. This result shows that a reliable description of 4-styrylpyridine with high-level post-HF methods requires a sufficiently flexible basis set, such as the aug-cc-pVDZ basis set (or an even larger one). For an accurate determination of the *cis*–*trans* energy difference within this theoretical framework, the

Table 9. Barrier heights $\Delta E_i^{\ddagger}$ [cm^{-1}] for the rotation of the pyridinyl group ($i=4$) and the phenyl group ($i=5$) in *cis*-4-styrylpyridine (see Figure 10). Selected distances [Å] and angles [°] characterizing the transition states are also given.

	$\Delta E_i^{\ddagger}$ [a]	C^{Ph}–C^1	C^1–C^2	C^2–C^{Py}	C^{Ph}–C^1–C^2	C^1–C^2–C^{Py}	τ	∢(Py,Ph)
TS_4: rotation of the pyridinyl group								
B3LYP/*G*	545	1.470	1.350	1.490	131.8	129.3	0.0	90.0
PBE/*G*	631	1.470	1.360	1.490	131.5	129.1	0.3	88.7
TS_5: rotation of the phenyl group								
B3LYP/*G*	541	1.490	1.350	1.480	129.2	131.0	0.1	89.7
PBE/*G*	625	1.490	1.360	1.470	128.9	130.7	0.3	88.9

[a] Not corrected from the zero-point vibrational contribution.

use of coupled cluster methods, for example, CCSD or preferably CCSD(T), would be highly desirable. However, for a system of moderate size, such as 4-styrylpyridine (25 atoms), the requirement of a sufficiently large basis set makes this approach intractable. Such a situation contrasts with that of the DFT methods and, indeed, for a computational cost comparable to that of the HF method, the use of conceptually distinct functionals (such as the B3LYP hybrid and the PBE GGA), with basis sets of very different qualities, helped us to obtain an equivalent and reliable description of 4-styrylpyridine at the *cis* and *trans* minima.

Calculations carried out at the B3LYP/*G* and PBE/*G* levels also allowed the characterization of 4-styrylpyridine at six transition states located on the ground-state PES. The molecule was thus characterized at the transition state TS_0 associated with the *cis*⇄*trans* isomerization process. At TS_0, 4-styrylpyridine is actually an OSS biradical and, as such, it could not be characterized within the restricted single-determinantal KS framework because the approximate functionals do not accurately account for the left–right correlation. We therefore used the BS approach, which provides a reliable solution to this problem. The results thus obtained with the two functionals are very consistent with each other. The geometry found for 4-styrylpyridine at TS_0 is that of a rotated alkene, and the height of the isomerization barrier, taken with respect to the energy of the *trans* isomer, amounts to $\Delta E_0^{\neq} \approx 15\,820\ cm^{-1}$ ($\Delta E_0^{\neq} \approx 45.2$ kcal mol^{-1}). The other five transitions states, TS_i ($i = 1,\ldots,5$), were determined from restricted calculations. The results obtained with the two functionals for any of these transition states were also very consistent with each other and can be summarized as follows: For the transition state TS_1, which is associated with the enantiomerization of the *cis* isomer, the calculated barrier height is $\Delta E_1^{\neq} \approx 1543\ cm^{-1}$ ($\Delta E_1^{\neq} \approx 4.4$ kcal mol^{-1}). The transition states TS_2 and TS_3 are associated, respectively, with the rotations of the phenyl and pyridinyl groups in the *trans* isomer, and the calculated barrier heights are $\Delta E_2^{\neq} \approx 1793\ cm^{-1}$ ($\Delta E_2^{\neq} \approx 5.1$ kcal mol^{-1}) and $\Delta E_3^{\neq} \approx 1741\ cm^{-1}$ ($\Delta E_3^{\neq} \approx 5.0$ kcal mol^{-1}). As for the transition states TS_4 and TS_5, these are associated, respectively, with the rotations of the pyridinyl and phenyl groups in the *cis* isomer, with barrier heights of $\Delta E_4^{\neq} \approx 588\ cm^{-1}$ ($\Delta E_4^{\neq} \approx 1.7$ kcal mol^{-1}) and $\Delta E_5^{\neq} \approx 584\ cm^{-1}$ ($\Delta E_5^{\neq} \approx 1.7$ kcal mol^{-1}). The rotation of either aromatic substituent in the *cis* isomer actually translates into the enantiomerization of this isomer.

We also performed CPMD simulations at 50, 150, and 300 K. The results of these simulations, performed at the PBE/*P* level, showed that the evolution of the molecule in the vicinity of the *cis* and *trans* minima is characterized by large fluctuations, whose amplitudes increase with temperature. This is particularly the case for the phenyl and pyridinyl moities, which (from the point of view of an observer sitting on the ethylenic fragments) undergo large and concerted clockwise–counterclockwise partial rotations about the single C–C bonds. This implies that the *trans* isomer mainly exists at finite temperatures in a nonplanar form. Incidentally, the simulation carried out at 150 K on the *cis* isomer allowed us to observe the complete rotation of the pyridiniyl ring, which took place within ≈1 ps. In summary, the present theoretical study of 4-styrylpyridine allowed us to gain significant insight into its ground-state geometrical and energetic properties as well as into its ground-state reactivity. A similar static and MD study is being carried out to investigate the photophysics and photochemistry of the molecule; the results will be reported elsewhere.

Acknowledgements

This work received financial support from the MAGMANet NoE of the European Union (contract NMP3-CT-2005-515767-2). We acknowledge computer time at the "Centro Svizzero di Calcolo Scientifico" (CSCS) and the "Centre Universitaire d'Informatique" (CUI) of the University of Geneva. We thank Andreas Hauser for the critical reading of the manuscript and helpful discussions. L.M.L.D. thanks the University of Versailles for a guest professor position.

Keywords: ab initio calculations · density functional calculations · isomerization · molecular dynamics · transition states

[1] D. Gegiou, K. A. Muszkat, E. Fischer, *J. Am. Chem. Soc.* **1968**, *90*, 3907–3918.
[2] *Photochromism, Molecules and Systems in Studies in Organic Chemistry* (Eds.: H. Dürr, H. Bouas-Laurent), Elsevier, Amsterdam, **1990**.
[3] H. Meier, *Angew. Chem.* **1992**, *104*, 1425–1446; *Angew. Chem. Int. Ed. Engl.* **1992**, *31*, 1399–1420.
[4] P. Rademacher, A. L. Marzinzik, K. Kowski, M. R. Weiß, *Eur. J. Org. Chem.* **2001**, 121–130.
[5] R. S. H. Liu, D. T. Browne, *Acc. Chem. Res.* **1986**, *19*, 42–48.
[6] C. H. Evans, J. Reynisson, J. K. F. Geirsson, A. Kvaran, W. P. McGimpsey, *J. Photochem. Photobiol. A* **1998**, *115*, 57–61.
[7] C. Bräuchle, N. Hampp, D. Oesterhelt, *Adv. Mater.* **1991**, *3*, 420–428.
[8] B. L. Feringa, W. F. Jager, B. de Lange, *Tetrahedron* **1993**, *49*, 8267–8310.
[9] P. P. Zarnegar, C. R. Bock, D. G. Whitten, *J. Am. Chem. Soc.* **1973**, *95*, 4367–4372.
[10] M. S. Wrighton, D. L. Morse, L. Pdungsap, *J. Am. Chem. Soc.* **1975**, *97*, 2073–2079.
[11] L. Pdungsap, M. S. Wrighton, *J. Organomet. Chem.* **1977**, *127*, 337–347.
[12] L. L. Costanzo, S. Giuffrida, G. De Guidi, G. Condorelli, *J. Photochem. Photobiol. A* **1998**, *46*, 295–300.
[13] J. Otsuki, A. Suka, K. Yamazaki, H. Abe, Y. Araki, O. Ito, *Chem. Commun.* **2004**, 1290–1291.
[14] H. Sugimoto, T. Kimura, S. Inoue, *J. Am. Chem. Soc.* **1999**, *121*, 2325–2326.
[15] H. Sugimoto, S. Inoue, *Pure Appl. Chem.* **1998**, *70*, 2365–2369.
[16] *Spin Crossover in Transition Metal Compounds I, Top. Curr. Chem., Vol. 233,* (Ed.: P. Gütlich, H. A. Goodwin), Springer, Heidelberg, **2004**.
[17] *Spin Crossover in Transition Metal Compounds II, Top. Curr. Chem., Vol 234,* (Ed.: P. Gütlich, H. A. Goodwin), Springer, Heidelberg, **2004**.
[18] *Spin Crossover in Transition Metal Compounds III, Top. Curr. Chem., Vol 235,* (Ed.: P. Gütlich, H. A. Goodwin), Springer, Heidelberg, **2004**.
[19] O. Kahn, *Molecular Magnetism*, VCH, Weinheim, **1993**.
[20] P. Gütlich, A. Hauser, H. Spiering, *Angew. Chem.* **1994**, *106*, 2109–2141; *Angew. Chem. Int. Ed. Engl.* **1994**, *33*, 2024–2054.
[21] M.-L. Boillot, J. Zarembowitch, A. Sour in *Spin Crossover in Transition Metal Compounds II, Top. Curr. Chem., Vol. 234* (Ed.: P. Gütlich, H. A. Goodwin), Springer, Heidelberg, **2004**, 261–276.
[22] C. Roux, J. Zarembowitch, B. Gallois, T. Granier, R. Claude, *Inorg. Chem.* **1994**, *33*, 2273–2279.
[23] M.-L. Boillot, C. Roux, J.-P. Audière, A. Dausse, J. Zarembowitch, *Inorg. Chem.* **1996**, *35*, 3975–3980.

[24] J. S. Kolb, M. D. Thomson, M. Novosel, K. Sénéchal, E. Rivière, M.-L. Boillot, H. Roskos. C. R. Chim. , *Compt. Rend. Chim.* **2007**, *10*, 1 – 10.
[25] T. D. Crawford, H. F. Schaefer III in *Reviews in Computational Chemistry, Vol. 14* (Eds.: K. B. Lipkowitz, D. B. Boyd), Wiley, New York, **2000**, pp. 33 – 136.
[26] K. Andersson, P.-Å. Malmqvist, B. O. Roos, A. J. Sadlej, K. Wolinski, *J. Phys. Chem.* **1990**, *94*, 5483 – 5488.
[27] K. Andersson, P.-Å. Malmqvist, B. O. Roos, *J. Chem. Phys.* **1992**, *96*, 1218 – 1226.
[28] P. Hohenberg, W. Kohn, *Phys. Rev.* **1964**, *136*, B864 – B871.
[29] W. Kohn, L. J. Sham, *Phys. Rev.* **1965**, *140*, A1133 – A1138.
[30] R. G. Parr, W. Yang, *Density Functional Theory of Atoms and Molecules*, Oxford University Press, New York, **1989**.
[31] R. M. Dreizler, E. K. U. Gross, *Density Functional Theory, An Approach to the Quantum Many-Body Problem*, Springer, Heidelberg, **1990**.
[32] W. Koch, M. C. Holthausen, *A Chemist's Guide to Density Functional Theory*, Wiley, New York, **2000**.
[33] A. Fouqueau, S. Mer, M. E. Casida, L. M. Lawson Daku, A. Hauser, T. Mineva, *J. Chem. Phys.* **2004**, *120*, 9473 – 9486.
[34] H. Paulsen, A. X. Trautwein, *J. Phys. Chem. Solids* **2004**, *65*, 793 – 798.
[35] A. Fouqueau, M. E. Casida, L. M. Lawson Daku, A. Hauser, F. Neese, *J. Chem. Phys.* **2005**, *122*, 044110.
[36] L. M. Lawson Daku, A. Vargas, A. Hauser, A. Fouqueau, M. E. Casida, *ChemPhysChem* **2005**, *6*, 1393 – 1410.
[37] G. Ganzenmüller, N. Berkaine, A. Fouqueau, M. E. Casida, M. Reiher, *J. Chem. Phys.* **2005**, *122*, 234321.
[38] A. Hauser, C. Enachescu, M. Lawson Daku, A. Vargas, N. Amstutz, *Coord. Chem. Rev.* **2006**, *250*, 1642 – 1652.
[39] I. Krivokapic, M. Zerara, M. Lawson Daku, A. Vargas, C. Enachescu, C. Ambrus, P. Tregenna-Piggott, N. Amstutz, E. Krausz, A. Hauser, *Coord. Chem. Rev.* **2007**, *251*, 364 – 378.
[40] A. Vargas, M. Zerara, E. Krausz, A. Hauser, L. M. Lawson Daku, *J. Chem. Theory Comput.* **2006**, *2*, 1342 – 1359.
[41] NWChem, version 4.7, E. Aprà, T. L. Windus, T. P. Straatsma, E. J. Bylaska, W. de Jong, S. Hirata, M. Valiev, M. Hackler, L. Pollack, K. Kowalski, R. Harrison, M. Dupuis, D. M. A. Smith, J. Nieplocha, V. Tipparaju, M. Krishnan, A. A. Auer, E. Brown, G. Cisneros, G. Fann, H. Früchtl, J. Garza, K. Hirao, R. Kendall, J. Nichols, K. Tsemekhman, K. Wolinski, J. Anchell, D. Bernholdt, P. Borowski, T. Clark, D. Clerc, H. Dachsel, M. Deegan, K. Dyall, D. Elwood, E. Glendening, M. Gutowski, A. Hess, J. Jaffe, B. Johnson, J. Ju, R. Kobayashi, R. Kutteh, Z. Lin, R. Littlefield, X. Long, B. Meng, T. Nakajima, S. Niu, M. Rosing, G. Sandrone, M. Stave, H. Taylor, G. Thomas, J. van Lenthe, A. Wong, Z. Zhang, Pacific Northwest National Laboratory, Richland, WA, USA, **2005**.
[42] R. A. Kendall, E. Aprà, D. E. Bernholdt, E. J. Bylaska, M. Dupuis, G. I. Fann, R. J. Harrison, J. Ju, J. A. Nichols, J. Nieplocha, T. P. Straatsma, T. L. Windus, A. T. Wong, *Comput. Phys. Commun.* **2000**, *128*, 260 – 283.
[43] A. D. Becke, *J. Chem. Phys.* **1993**, *98*, 1372 – 1377.
[44] A. D. Becke, *J. Chem. Phys.* **1993**, *98*, 5648 – 5652.
[45] *Gaussian NEWS*, vol. 5, no. 2, summer **1994**, p. 2. "Becke3LYP Method References and General Citation Guidelines".
[46] J. P. Perdew, K. Burke, M. Ernzerhof, *Phys. Rev. Lett.* **1996**, *77*, 3865 – 3868.
[47] J. P. Perdew, K. Burke, M. Ernzerhof, *Phys. Rev. Lett.* **1997**, *78*, 1396.
[48] N. Godbout, D. R. Salahub, J. Andzelm, E. Wimmer, *Can. J. Chem.* **1992**, *70*, 560 – 571.
[49] T. H. Dunning, Jr., *J. Chem. Phys.* **1989**, *90*, 1007 – 1023.
[50] R. A. Kendall, T. H. Dunning, Jr., *J. Chem. Phys.* **1992**, *96*, 6796 – 6806.
[51] D. E. Woon, T. H. Dunning, Jr., *J. Chem. Phys.* **1993**, *98*, 1358 – 1371.
[52] R. Car, M. Parinello, *Phys. Rev. Lett.* **1985**, *55*, 2471 – 2474.
[53] *CPMD*, Copyright IBM Corp. (**1990**–**2006**), Copyright MPI für Festkörperforschung Stuttgart (**1997**–**2001**).
[54] L. Kleinman, D. M. Bylander, *Phys. Rev. Lett.* **1982**, *48*, 1425 – 1428.
[55] N. Troullier, J. Luriaas Martins, *Phys. Rev. B* **1991**, *43*, 1993 – 2006.
[56] G. J. Martyna, M. E. Tuckerman, *J. Chem. Phys.* **1999**, *110*, 2810 – 2821.
[57] S. Nosé, *Mol. Phys.* **1984**, *52*, 255 – 268.
[58] S. Nosé, *J. Chem. Phys.* **1984**, *81*, 511 – 519.
[59] W. G. Hoover, *Phys. Rev. A* **1985**, *31*, 1695 – 1697.
[60] G. J. Martyna, M. L. Klein, M. Tuckerman, *J. Chem. Phys.* **1992**, *97*, 2635 – 2643.
[61] M. E. Tuckerman, M. Parrinello, *J. Chem. Phys.* **1994**, *101*, 1302 – 1315.
[62] G. J. Martyna, M. E. Tuckerman, D. J. Tobias, M. L. Klein, *Mol. Phys.* **1996**, *87*, 1117 – 1157.
[63] Ecce, A Problem Solving Environment for Computational Chemistry, version 3.2.4, G. Black, B. Didier, T. Elsethagen, D. Feller, D. Gracio, M. Hackler, S. Havre, D. Jones, E. Jurrus, T. Keller, C. Lansing, S. Matsumoto, B. Palmer, M. Peterson, K. Schuchardt, E. Stephan, L. Sun, H. Taylor, G. Thomas, E. Vorpagel, T. Windus, C. Winters, Pacific Northwest National Laboratory, Richland, WA, USA, **2005**.
[64] L. Laaksonen, *J. Mol. Graph.* **1992**, *10*, 33 – 34.
[65] D. L. Bergman, L. Laaksonen, A. Laaksonen, *J. Mol. Graphics Modell.* **1997**, *15*, 301 – 306.
[66] E. Cariati, D. Roberto, R. Ugo, V. I. Srdanov, S. Galli, P. Macchi, A. Sironi, *New J. Chem.* **2002**, *26*, 13 – 15.
[67] G. Marconi, G. Bartocci, U. Mazzucato, A. Spalletti, F. Abbate, L. Angeloni, E. Castellucci, *Chem. Phys.* **1995**, *196*, 383 – 393.
[68] K. Ogawa, H. Suzuki, M. Futakami, *J. Chem. Soc. Perkin Trans. 2* **1988**, 39 – 43.
[69] B. B. Champagne, J. F. Pfanstiel, D. F. Plusquellic, D. W. Pratt, W. M. van Herpen, W. L. Meerts, *J. Phys. Chem.* **1990**, *94*, 6 – 8.
[70] S. P. Kwasniewski, L. Claes, J.-P. François, M. S. Deleuze, *J. Chem. Phys.* **2003**, *118*, 7823 – 7836.
[71] E. L. Eliel, J. Engelsman, *J. Chem. Educ.* **1996**, *73*, 903 – 905.
[72] D. G. Whitten, Y. J. Lee, *J. Am. Chem. Soc.* **1972**, *94*, 9142 – 9148.
[73] U. Mazzucato, *Gazz. Chim. Ital.* **1987**, *117*, 661 – 665.
[74] F. Barigelletti, S. Dellonte, G. Orlandi, G. Bartocci, F. Masetti, U. Mazzucato, *J. Chem. Soc. Faraday Trans. 1* **1984**, 1123 – 1129.
[75] W.-G. Han, T. Lovell, T. Liu, L. Noodleman, *ChemPhysChem* **2002**, *3*, 167 – 178.
[76] L. Salem, C. Rowland, *Angew. Chem.* **1972**, *84*, 86 – 106; *Angew. Chem. Int. Ed. Engl.* **1972**, *11*, 92 – 111.
[77] L. Salem, *Electrons in Chemical Reactions: First Principles*, Wiley, New York, **1982**.
[78] J. Michl, V. Bonačić-Koutecký, *Electronic Aspects of Organic Photochemistry*, Wiley, New York, **1990**.
[79] M. H. Lim, S. E. Worthington, F. J. Dulles, C. J. Cramer in *Density Functional Methods in Chemistry, Vol. 629 of ACS Symposium Series* (Eds.: B. B. Laird, R. B. Ross, T. Ziegler), American Chemical Society, Washington DC, **1996**, p. 402.
[80] M. Filatov, S. Shaik, *Chem. Phys. Lett.* **1999**, *304*, 429437.
[81] J. Gräfenstein, A. M. Hjerpe, E. Kraka, D. Cremer, *J. Phys. Chem. A* **2000**, *104*, 1748 – 1761.
[82] J. Gräfenstein, E. Kraka, M. Filatov, D. Cremer, *Int. J. Mol. Sci.* **2002**, *3*, 360 – 394.
[83] M. H. Matus, R. Contreras, A. Cedillo, M. Galván, *J. Chem. Phys.* **2003**, *119*, 4112 – 4116.
[84] O. V. Gritsenko, P. R. T. Schipper, E. J. Baerends, *J. Chem. Phys.* **1997**, *107*, 5007 – 5015.
[85] P. R. T. Schipper, O. V. Gritsenko, E. J. Baerends, *J. Chem. Phys.* **1999**, *111*, 4056 – 4067.
[86] O. V. Gritsenko, B. Ensing, P. R. T. Schipper, E. J. Baerends, *J. Phys. Chem. A* **2000**, *104*, 8558 – 8565.
[87] N. C. Handy, A. J. Cohen, *Mol. Phys.* **2001**, *99*, 403 – 412.
[88] E. J. Baerends, *Phys. Rev. Lett.* **2001**, *87*, 133004.
[89] A. D. Becke, *J. Chem. Phys.* **2003**, *119*, 2972 – 2977.
[90] It is worth mentioning here that the *trans*→*cis* isomerization can lead to the formation of either the Λ or the Δ enantiomer. This is of importance for the stereochemistry of a complex such as Fe(*cis*-4-styrylpyridine)$_4$(NCS)$_2$ when obtained from an LD-LISC experiment.
[91] E. R. Johnson, R. A. Wolkow, G. A. DiLabio, *Chem. Phys. Lett.* **2004**, *394*, 334 – 338.

Received: February 16, 2007
Published online on May 25, 2007

